Soft Matter

Accepted Manuscript

This is an *Accepted Manuscript*, which has been through the Royal Society of Chemistry peer review process and has been accepted for publication.

Accepted Manuscripts are published online shortly after acceptance, before technical editing, formatting and proof reading. Using this free service, authors can make their results available to the community, in citable form, before we publish the edited article. We will replace this *Accepted Manuscript* with the edited and formatted *Advance Article* as soon as it is available.

You can find more information about *Accepted Manuscripts* in the Information for Authors.

Please note that technical editing may introduce minor changes to the text and/or graphics, which may alter content. The journal's standard Terms & Conditions and the Ethical guidelines still apply. In no event shall the Royal Society of Chemistry be held responsible for any errors or omissions in this *Accepted Manuscript* or any consequences arising from the use of any information it contains.

ROYAL SOCIETY OF CHEMISTRY

www.rsc.org/softmatter

Preparation, characterization and magnetic behavior of a spin-labelled physical hydrogel containing a chiral cyclic nitroxide radical unit fixed inside the gelator molecule

Yusa Takemoto,[1] Takayuki Yamamoto,[1] Naohiko Ikuma,[2] Yoshiaki Uchida,[3,4] Katsuaki Suzuki,[1] Satoshi Shimono,[1] Hiroki Takahashi,[1] Nobuhiro Sato,[5] Yojiro Oba,[5] Rintaro Inoue,[5] Masaaki Sugiyama,[5] Hirohito Tsue,[1] Tatsuhisa Kato,[1] Jun Yamauchi,[1] Rui Tamura*[1]

[1]Graduate School of Human and Environmental Studies, Kyoto University, Kyoto 606-8501, Japan
[2]Graduate School of Engineering, Osaka University, Suita, Osaka 565-0871, Japan
[3]Graduate School of Engineering Science, Osaka University, Toyonaka, Osaka 560-8531, Japan
[4]Japan Science and Technology Agency, PRESTO, 4-1-8 Honcho, Kawaguchi, Saitama 332-0012, Japan
[5]Research Reactor Institute, Kyoto University, Osaka 590-0494, Japan

Abstract

An optically active amphiphilic nitroxide radical compound [(*S*,*S*,*R*)-**5a**], which contains a paramagnetic (2*S*,5*S*)-2,5-dimethyl-2,5-diphenylpyrrolidine-*N*-oxyl radical group fixed in the inner position together with a hydrophobic long alkyl chain and a hydrophilic (*R*)-alanine residue in the opposite terminal positions, was found to serve as a low-molecular-weight gelator in H_2O to give rise to a spin-labelled physical hydrogel. Characterization of the hydrogel was performed by microscopic (SEM, TEM and AFM) techniques, XRD and SAXS measurements, and IR, UV and CD spectroscopies. The gel–sol transition temperature was determined by EPR spectral line-width (ΔH_{pp}) analysis. Measurement of the temperature dependence of relative paramagnetic susceptibility (χ_{rel}) for the hydrogel and sol phases was achieved by means of the double-integration of VT-EPR spectra.

Keywords: electron paramagnetic resonance (EPR) spectroscopy, gel, sol, nitroxide radical, magnetic physical hydrogel

1 Introduction

Amongst persistent organic open-shell compounds such as nitroxides, verdazyls, thioaminyls, a certain hydrazyl, phenoxyls, and trityl radicals, nitroxide radicals show

Soft Matter Accepted Manuscript

outstanding thermodynamic stability ascribed to the delocalization of the unpaired electron over the N–O bond and thereby no dimerization or recombination.[1] For this reason, since the discovery of the purely organic ferromagnet (critical temperature, *T*c = 0.6 K) with respect to one of several polymorphs of 2-(4-nitrophenyl)-4,4,5,5-tetramethylimidazoline-1-oxy-3-oxide (**1**) (Fig. 1),[2] nitroxide radical structures have been used as the spin source to develop metal-free solid state magnetic materials and spintronic devices.[3-9] Up to the late 1990s, more than twenty nitroxide radical-based organic ferromagnets were prepared;[10] the highest *T*c of 1.48 K was recorded for one of polymorphs of 1,3,5,7-tetramethyl-2,6-diazaadamatane-*N*,*N*'-dioxyl (**2**).[11] However, these organic nitoxide radical crystals showed a paramagnetic behavior above the *T*c.

Different from paramagnetic organic nitroxide radical crystals,[1,10] metal-free paramagnetic soft materials are expected to exhibit a unique dynamic magnetic behavior induced by applied magnetic fields at high temperatures, which originates from inhomogeneous intermolecular contacts due to the swift molecular motion and coherent collective properties of molecules in the soft phases.[12-17] For example, all-organic rod-like liquid crystalline (LC) materials (**3**) with a stable nitroxide radical unit in the central core portion and a negative dielectric anisotropy ($\Delta\varepsilon < 0$) were found to exhibit a sort of spin glass-like inhomogeneous ferromagnetic interactions (average spin-spin exchange interaction constant $\bar{J} > 0$) induced by weak magnetic fields in various chiral and achiral LC phases at high temperatures (30-150 °C).[18-22] Indeed, these radical LC droplets floating on water were attracted to a weak permanent magnet and moved swiftly under the influence of the magnet. The origin of such unique magnetic interactions, which were referred to as positive 'magneto-LC effects',[20] were interpreted in terms of the preferential occurrence of ferromagnetic spin-spin dipole interactions in magnetic fields due to the inhomogeneous intermolecular contacts in the LC phases.[19-21] Furthermore, by EPR studies and DFT calculations Vorobiev *et al.* revealed that the spin polarization mechanism between neighboring radical molecules rather than the direct through-space interactions between paramagnetic centers contributes to the occurrence of the positive magneto-LC effects.[23]

Soft Matter Accepted Manuscript

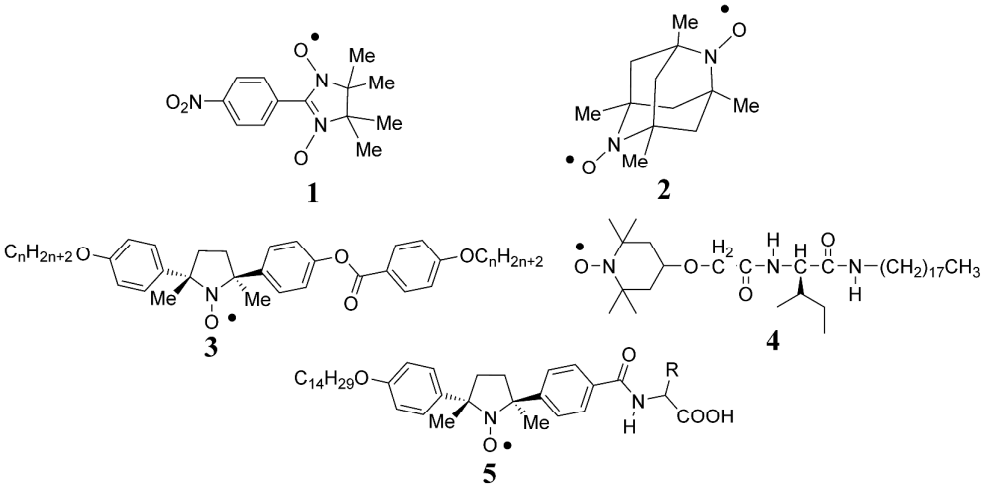

Fig. 1 Molecular structures of nitroxide radical compounds **1-5**.

From these results it is expected that analogous magnetic interactions may be induced by weak magnetic fields in other metal-free magnetic soft materials, such as gels, which show a high sensitivity to external heat, pressure, light, pH and so forth.[24-27] Since the first report on organogelation of a nitroxide radical-labelled steroid in cyclohexane,[28] three spin-labelled gelators bearing a 2,2,6,6-tetramethyl-1-piperidinyloxy (TEMPO) radical pendant in the terminal position of molecules have been reported.[29-31] Interestingly, Kato *et al*. revealed the paramagnetic behavior with weak antiferromagnetic interactions with respect to the radical moieties aligned one-dimensionally on the L-isoleucine-based β-sheet scaffold of gelator **4** by superconducting quantum interference device (SQUID) measurements of the physical organogels in the presence of organic solvents in the temperature range of 2 to 240 K.[29] However, there has been no precedent concerning magnetic gels containing a radical unit or a paramagnetic metal ion in the central position of a molecule.

With this situation in mind, according to the general molecular design of gelators,[24-27] we have designed and synthesized three optically active amphiphilic radical compounds **5** [(*S*,*S*,*R*)-**5a** with (*R*)-Ala, (*S*,*S*,*S*)-**5b** with (*S*)-Ala, and (*S*,*S*)-**5c** with Gly (Fig. 2)] with negative dielectric anisotropy ($\Delta\varepsilon < 0$) (Fig. S1) as candidates for a hydrogelator, which consist of a (2*S*,5*S*)-2,5-dimethyl-2,5-diphenylpyrrolidine-*N*-oxyl radical group as the spin source fixed in the inner position, and a long alkyl chain and an amino acid residue as the hydrophobic and hydrophilic functionalities, respectively, in the opposite terminal positions. Here we report the preparation and characterization of the hydrogel of (*S*,*S*,*R*)-**5a** and the magnetic behavior observed in the gel and sol states clarified by

Soft Matter Accepted Manuscript

variable temperature electron paramagnetic resonance (VT-EPR) spectroscopy.

2 Experimental

2.1 Preparation of (*S*,*S*,*R*)-5a

4-(4,6-Dimethoxy-1,3,5-triazin-2-yl)-4-methylmorpholinium chloride (DMT-MM, 76.1 mg, 0.275 mmol) was added to a solution of (*S*,*S*)-4-[5-(4-tetradecyloxyphenyl)-2,5-dimethylpyrrolidine-1-oxyl-2-yl]benzoic acid (144 mg, 0.275 mmol) and *N*-methylmorpholine (8.34 mg, 0.083 mmol) in acetone/CH_2Cl_2 (1.5 mL/0.5 mL) at 25 °C. After stirring for 15 min, a solution of (D)-(*R*)-Alanine (27.0 mg, 0.303 mmol) and potassium carbonate (41.8 mg, 0.303 mmol) in water (0.5 mL) was added, and the mixture was stirred for 12 h at 25 °C. The aqueous phase was acidified with 5 w% H_2SO_4 to pH 2-4, and extracted with CH_2Cl_2 (15 ml) three times. The combined organic layer was dried over $MgSO_4$, filtered and the solvent was evaporated under reduced pressure. The residual solid was purified by flash column chromatography on silica gel (9:1 $CHCl_3$/ether) to give 102 mg (63%) of (*S*,*S*,*R*)-**5a** as a yellow amorphous solid. (*S*,*S*,*R*)-**5a** (82% *de*): IR (KBr) 3446, 2976, 2922, 2852, 2372, 2345, 1791, 1560, 1462, 1290, 1250, 897, 774 cm^{-1}. $[\alpha]_D^{25}$ = –95.8 (c 0.20, THF). Anal. Calcd for $C_{36}H_{53}N_2O_5$: C, 72.81; H, 9.00; N, 4.72. Found: C, 72.57; H, 9.07; N, 4.47.

Similarly, (*S*,*S*,*S*)-**5b** and (*S*,*S*)-**5c** were prepared in 69% and 70% yields, respectively, as yellow solids. (*S*,*S*,*S*)-**5b** (85% *de*): m.p. 143.3 °C (DSC); IR (KBr) 3446, 2976, 2922, 2852, 2372, 2345, 1791, 1560, 1462, 1290, 1250, 897, 774 cm^{-1}. Anal. Calcd for $C_{36}H_{53}N_2O_5$: C, 72.81; H, 9.00; N, 4.72. Found: C, 72.91; H, 8.91; N, 4.65. $[\alpha]_D^{25}$ = –79.0 (c 0.20, THF). (*S*,*S*)-**5c** (82% *ee*): m.p. 113.9 °C (DSC); IR (KBr) 3446, 2976, 2922, 2852, 2372, 2345, 1791, 1560, 1462, 1290, 1250, 897, 774 cm^{-1}. Anal. Calcd for $C_{35}H_{51}N_2O_5$: C, 72.50; H, 8.87; N, 4.83. Found: C, 72.43; H, 8.88; N,4.83. $[\alpha]_D^{25}$ = –84.4 (c 0.20, THF).

2.2 Determination of *de* and *ee* values of 5a—5c

HPLC analysis was carried out using a chiral stationary phase column (Daicel Chiralpak OD-H, 0.46 cm × 25 cm) at 30 °C, a mixture of hexane, 2-propanol and TFA (700:300:5) as the mobile phase at the flow rate of 0.5 ml/min and a UV-vis spectrometer (254 nm) as the detector (Fig. S2).

2.3 X-ray crystallographic analysis of (*S*,*S*,*S*)-5b

Soft Matter Accepted Manuscript

X-ray intensity data were collected on a Rigaku Saturn724+ CCD area detector diffractometer mounted on a 1/4 χ goniometer [graphite-monochromated MoKα radiation (λ = 0.71073 Å); ω scans] at 100 K with a Rigaku low-temperature equipment. The crystal structure was solved by direct methods using SIR97[32] and refined on F^2 with all data using SHELXL97.[33] All non-hydrogen atoms were refined anisotropically, and hydrogen atoms were placed at calculated positions. All the crystallographic calculations were carried out using Yadokari XG-2009.[34]

Crystal data for (*S*,*S*,*S*)-**5b**: $C_{36}H_{53}N_2O_5$, M = 593.80, orthorhombic, a = 9.576(3) Å, b = 13.430(4) Å, c = 26.522(8) Å, V = 3410.9(18) Å^3, T = 100(2) K, space group $P2_12_12_1$, Z = 4, μ = 0.076 mm^{-1}, 27817 reflections measured, 7813 independent reflections (R_{int} = 0.0881). The final R_1 and $wR(F^2)$ values were 0.0822 ($I > 2\sigma(I)$) and 0.1262 ($I > 2\sigma(I)$), respectively. The final R_1 and $wR(F^2)$ values were 0.1132 (all data) and 0.1397 (all data), respectively. The goodness of fit on F^2 was 1.095. Crystallographic data have been deposited at the Cambridge Crystallographic Data Centre, 12 Union Road, 129 Cambridge CB2 1EZ, UK, and copies can be obtained on request, free of charge, by quoting the publication citation and the deposition number CCDC 1041193.

2.4 Preparation of the hydrogel of (*S*,*S*,*R*)-5a

In a 4 mL glass vial, 6.0 mg (1.0×10^{-2} mmol) of (*S*,*S*,*R*)-**5a** were dispersed in water (168 μL). The mixture (3.4 wt%) was heated at 80 °C using a water bath until the solid was dissolved. The resultant clear solution was then cooled down to room temperature. The hydrogel was formed in a few minutes. The gelation test was carried out by the test-tube inversion method.[24] The xerogel was obtained by freeze-drying the hydrogel.

2.5 Small angle X-ray scattering (SAXS) measurement of the hydrogel, xerogel and powder sample of (*S*,*S*,*R*)-5a (Fig. 7b)

SAXS camera (SAXES) installed at BL10C of KEK-PF (Ibaraki, Japan) was used to collect SAXS intensity data. SAXS intensities of samples were measured with an PILATUS 2M detector with an exposure time of 60 sec and a sample-to-detector distance of 2000 mm, which was calibrated by the powder diffraction from silver docosanoate. Circular averaging of the SAXS intensity data was then performed to obtain the one-dimensional intensity data I(q) as a function of q ($q = 4\pi \sin\theta/\lambda$, where 2θ is the scattering angle and the X-ray wavelength λ = 1.488 Å).

3 Results and Discussion

Soft Matter Accepted Manuscript

3.1 Preparation and characterization of hydrogel

Compounds (*S*,*S*,*R*)-**5a** (82% *de*), (*S*,*S*,*S*)-**5b** (85% *de*) and (*S*,*S*)-**5c** (82% *ee*) were synthesized from the precursor (*S*,*S*)-4-[5-(4-tetradecyloxyphenyl)-2,5-dimethylpyrrolidine-1-oxyl-2-yl]benzoic acid[35-37] as shown in Figure 2.

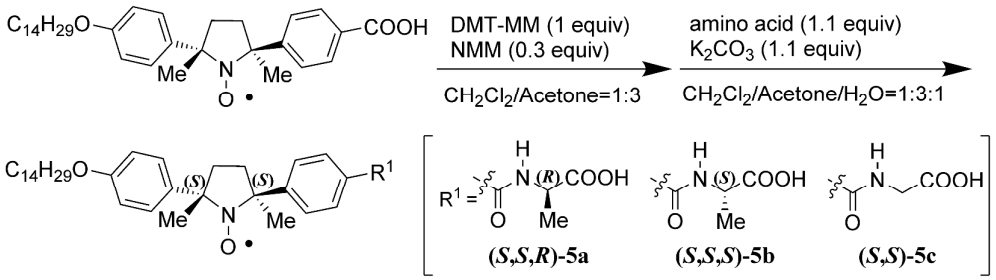

Fig. 2 Synthesis of (*S*,*S*,*R*)-**5a**, (*S*,*S*,*S*)-**5b** and (*S*,*S*)-**5c**.

First we found that (*S*,*S*,*R*)-**5a**, (*S*,*S*,*S*)-**5b**, and (*S*,*S*)-**5c** did not form an organogel with various organic solvents. Then we measured the solubility of amorphous (*S*,*S*,*R*)-**5a** and crystalline (*S*,*S*,*S*)-**5b** and (*S*,*S*)-**5c** in H_2O at 25 °C and evaluated the hydrogelation ability by heating the aqueous solutions followed by cooling (Fig. 3). Interestingly, of these three compounds, a semitransparent hydrogel was formed from (*S*,*S*,*R*)-**5a**, whereas crystals were precipitated for (*S*,*S*,*S*)-**5b** and (*S*,*S*)-**5c**. The hydrogel of (*S*,*S*,*R*)-**5a** was stable for more than one month and the gel–sol conversion was thermally reversible. The homologues of (*S*,*S*,*R*)-**5a**, which have a shorter C_8 or C_{12} alkyl chain, failed to form a hydrogel or provided an unstable hydrogel, respectively. The critical gelation concentration (CGC) of (*S*,*S*,*R*)-**5a** was 3.4 wt% (6.0 x 10^{-2} mol/L) in H_2O at 25 °C. The block-like single crystal of diastereomeric (*S*,*S*,*S*)-**5b** suitable for X-ray crystallographic analysis was obtained by recrystallization from the saturated aqueous ethanol solution (H_2O/EtOH, 1/5 v/v). The crystal structure of (*S*,*S*,*S*)-**5b** consists of homochiral 1D chains formed by the hydrogen bond between the amide carbonyl oxygen atom and the carboxyl group, but there is no hydrophobic interaction between long alkyl chains (Fig. 4). In this context, Fuhrhop *et al.* reported that the gelation behavior depends on the stereochemistry of gelators; some diastereomers dissolved in solvents to form gels but the others precipitated.[38] Since the gelation process is a delicate balance between dissolution and precipitation,[24-27] the rational explanation for hydrogel or crystal formation in our case is unclear at present.

Soft Matter Accepted Manuscript

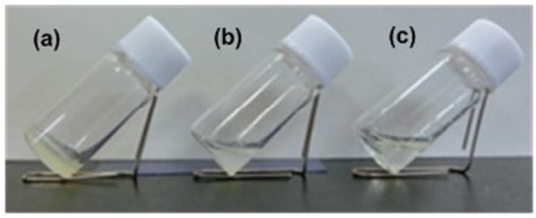

Compound	Solubility in H_2O at 25 °C	Gelation & CGC
(*S*,*S*,*R*)-**5a**	4.50 mg/mL (7.58×10^{-3} mol/L)	*yes* 3.4 wt% (6.0×10^{-2} mol/L)
(*S*,*S*,*S*)-**5b**	0.160 mg/mL (2.69×10^{-4} mol/L)	*no*
(*S*,*S*)-**5c**	0.120 mg/mL (2.07×10^{-4} mol/L)	*no*

Fig. 3 Comparison of hydrogelation abilities of (a) (*S*,*S*,*R*)-**5a**, (b) (*S*,*S*,*S*)-**5b** and (c) (*S*,*S*)-**5c** by heating at 80 °C followed by cooling to 25 °C.

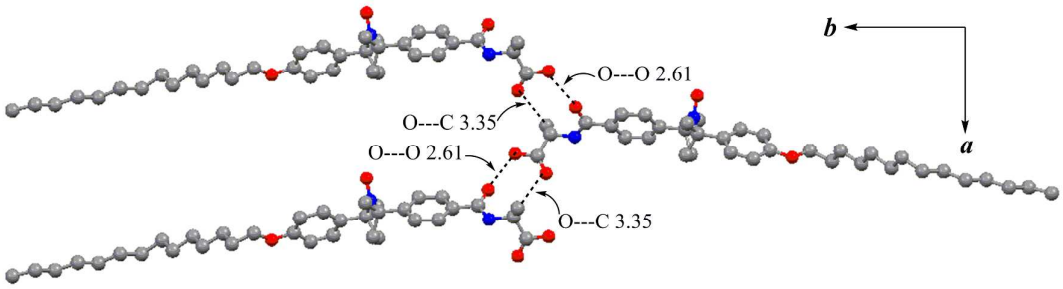

Fig. 4 X-ray crystal structure of (*S*,*S*,*S*)-**5b**. Homochiral 1D chain structure formed by the hydrogen bond (O---O 2.61 Å) between the amide carbonyl oxygen atom and the carboxyl group on the *ab* plane.

In order to verify the self-assembly of gelator molecules in the hydrogel of (*S*,*S*,*R*)-**5a**, the xerogel obtained from the hydrogel was subjected to microscopic (SEM, TEM, and AFM) observation (Figs. 5 and 6). The xerogel obtained from the hydrogel of (*S*,*S*,*R*)-**5a** (6.0×10^{-2} mol/L) by lyophilization and the nanofibers formed by evaporation of the aqueous solution (1.0×10^{-2} mol/L) of (*S*,*S*,*R*)-**5a** were subjected to SEM observation, and the samples for TEM observation were obtained by evaporation of the diluted aqueous solutions (1.0×10^{-2} and 5.0×10^{-3} mol/L) on 200-mesh copper grids coated with a perforated carbon film (Fig. 5). The SEM images of the xerogel showed the 3D network of nanofibers (Fig. 5a, b). Moreover, the formation of nanofibers of 100 to 300 nm in width was also confirmed by the TEM observation (Fig. 5c, d). To estimate the average aspect ratio of the nanofibers, the samples for AFM observation were prepared by spreading a small amount (~20 μL) of the hydrogel on a freshly cleaved

Soft Matter Accepted Manuscript

mica, followed by spontaneous evaporation. The AFM image of the resulting xerogel clearly demonstrated the formation of fibrous assembly of (*S*,*S*,*R*)-**5a** with no helical structure (Fig. 6a). Measurement of the height profile of nanofibers indicated that the average height-to-width ratio was ca. 1:3 (Fig. 6b).

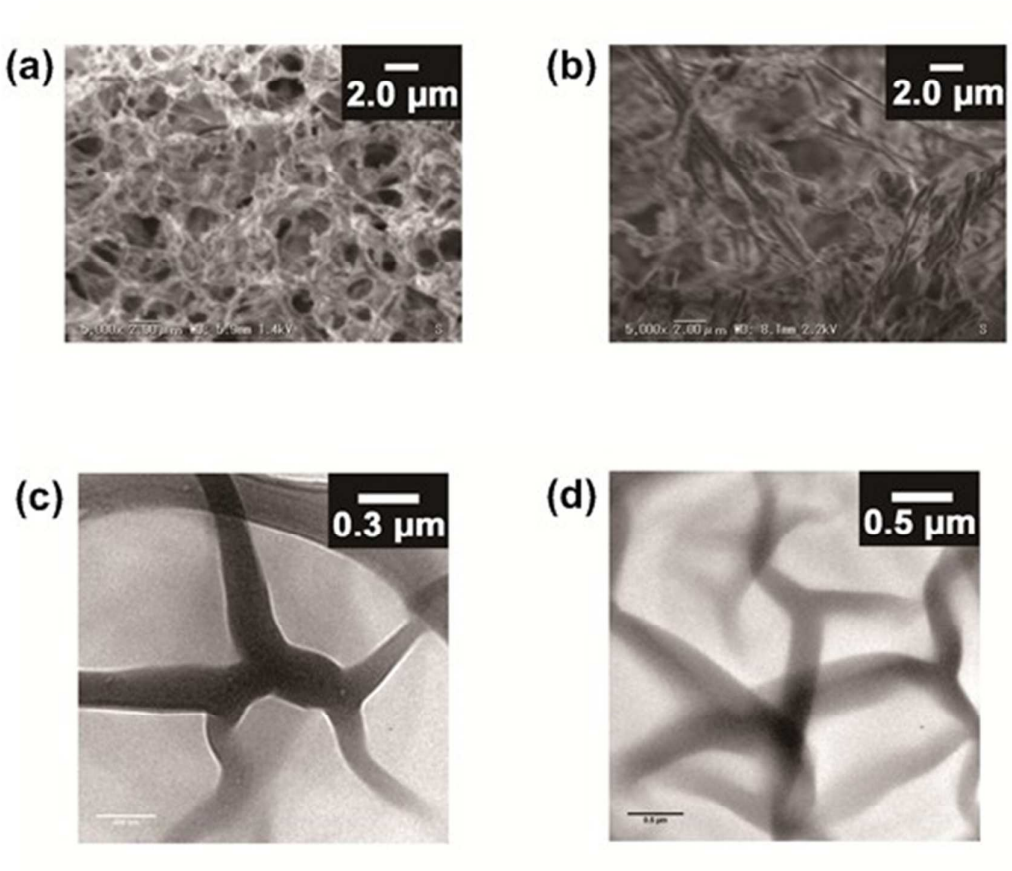

Fig. 5 SEM and TEM images of fibrous assembly of (*S*,*S*,*R*)-**5a**. SEM images of (a) the xerogel obtained from the hydrogel (6.0×10^{-2} mol/L) and (b) the nanofibers obtained by evaporation of the aqueous solution (1.0×10^{-2} mol/L). TEM images of the nanofibers obtained by evaporation of the aqueous solutions of (c) 1.0×10^{-2} mol/L and (d) 5.0×10^{-3} mol/L.

Soft Matter Accepted Manuscript

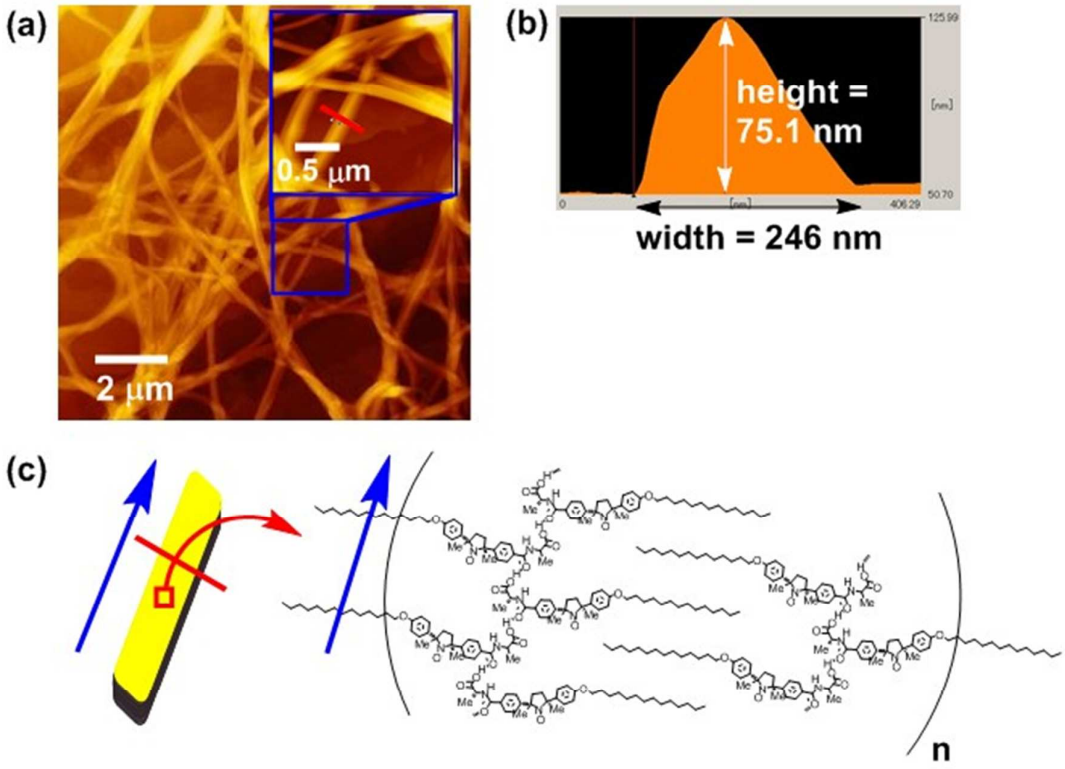

Fig. 6 Fibrous assembly in the xerogel of (*S*,*S*,*R*)-**5a**. (a) AFM image. (b) Height profile along the red line in the inset of image (a). (c) Speculated molecular arrangement in the nanofiber of (*S*,*S*,*R*)-**5a**.

To examine what kind of intermolecular interaction makes a big contribution to the formation of nanofibers, the solid-state IR spectrum of (*S*,*S*,*R*)-**5a** was compared with that of (*S*,*S*,*S*)-**5b**. The IR spectra of the powder sample of (*S*,*S*,*R*)-**5a** and the xerogel obtained from the hydrogel of (*S*,*S*,*R*)-**5a**, both of which did not show the out-of-plane bending vibration band near 920 cm^{-1} characteristic of dimeric carboxylic acids,[39] were very similar to that of the powder sample of (*S*,*S*,*S*)-**5b** (Fig. S3). Accordingly, the homochiral 1D chain structure between the amide oxygen atom and the carboxylic acid observed in the crystal structure of (*S*,*S*,*S*)-**5b** (Fig. 4) is also assumed to exist in the self-assembled nanofibers of (*S*,*S*,*R*)-**5a** (Fig. 6c).

To confirm the existence of periodic structures in the nanofibers, the xerogel and hydrogel of (*S*,*S*,*R*)-**5a** were subjected to the X-ray diffraction (XRD) and the small angle X-ray scattering (SAXS) measurements, respectively. Consequently, the XRD pattern of the xerogel showed two peaks at $2\theta = 1.9°$ (d = 46.5 Å) and 21.4° (4.2 Å) (Fig. 7a). Interestingly, a similar peak at 47.2 Å was observed in the SAXS patterns of

Soft Matter Accepted Manuscript

the gel and xerogel (Fig. 7b), indicating the existence of the same periodic structure. The 4.2 Å is most likely to correspond to either the mean distance between two alkyl chains or that of π-π stacked aromatic rings,[40] while 46.5 Å or 47.2 Å is shorter than twice as long as the molecular length (32 Å) of (*S*,*S*,*R*)-**5a** (Fig. S1) which was obtained by the AM1 Molecular Orbital calculations of the virtual molecular structure of (*S*,*S*,*R*)-**5a** derived from the crystal structure of (*S*,*S*,*S*)-**5b** (Fig. 4), suggesting the formation of interdigitated structure generated by hydrophobic intermolecular interactions of long alkyl chains (Fig. 6c). On the contrary, in the cases of (*S*,*S*,*S*)-**5b** and most likely (*S*,*S*)-**5c**, such interactions between long alkyl chains were not formed due to the different chirality of amino acid moieties, but instead stable crystals were produced (Fig. 4).

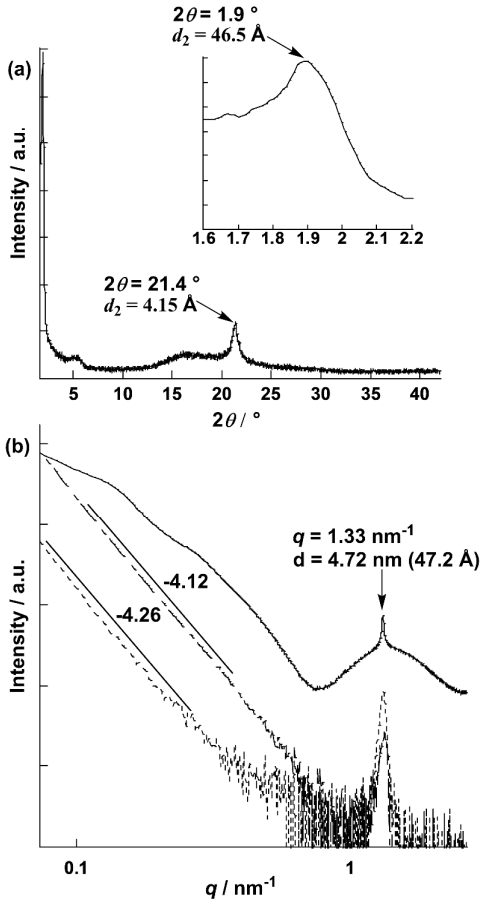

Fig. 7 (a) XRD pattern of the xerogel of (*S*,*S*,*R*)-**5a**. (b) SAXS patterns of (*S*,*S*,*R*)-**5a**; hydrogel (6.0 x 10^{-2} mol/L) (solid line, ——), xerogel (dashed line, — - —), and powder (broken line, – – –).

Soft Matter Accepted Manuscript

Furthermore, the intensities of UV absorption and CD cotton effects observed at 230 nm arising from the ^1L_a transition of C_6H_5-CO-$NHCH_3$ and CH_3O-C_6H_5[41,42] in the concentration of 1.0 x 10^{-4} mol/L of (*S*,*S*,*R*)-**5a** in H_2O were three times higher than those of 5.0 x 10^{-5} mol/L (Figure 8b, d), suggesting the self-assembly of gelator molecules in H_2O. In contrast, such a nonlinearity in the UV and CD spectral intensity was not observed in THF (Fig. 8a, c). These results were in good agreement with those from the EPR spectral studies; only broad singlet peak due to the self-assembly of gelator molecules was observed in a highly diluted aqueous solution of (*S*,*S*,*R*)-**5a** (1.0 x 10^{-4} mol/L), whereas only three-line shape spectrum due to the free molecule was observed at a higher concentration of 1.0 x 10^{-2} mol/L in THF (Fig. 9).

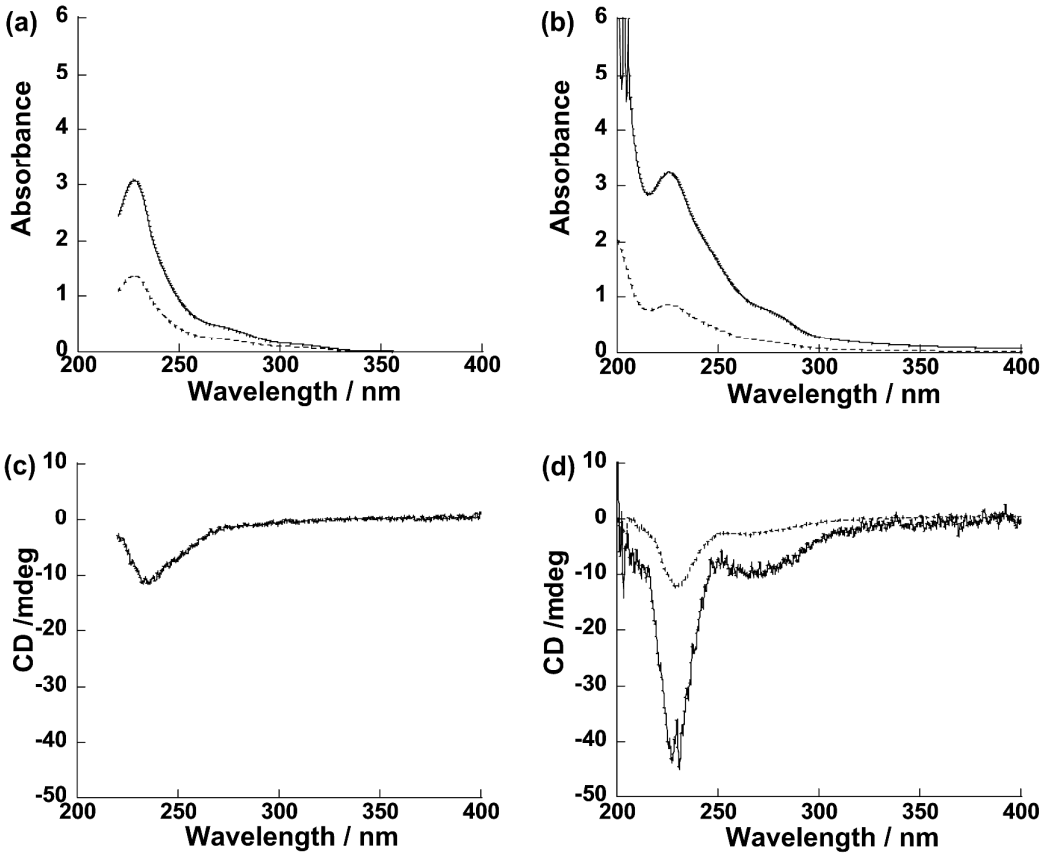

Fig. 8 UV (a and b) and CD (c and d) spectra in solutions of (*S*,*S*,*R*)-**5a** at 25 °C using a quartz cell with a path length of 10 mm. (a) 1.0 x 10^{-4} mol/L (solid line) and 5.0 x 10^{-5} mol/L (broken line) in THF. (b) 1.0 x 10^{-4} mol/L (solid line) and 5.0 x 10^{-5} mol/L (broken line) in H_2O. (c) 1.0 x 10^{-4} mol/L in THF. (d) 1.0 x 10^{-4} mol/L (solid line) and 5.0 x 10^{-5} mol/L (broken line) in H_2O.

Soft Matter Accepted Manuscript

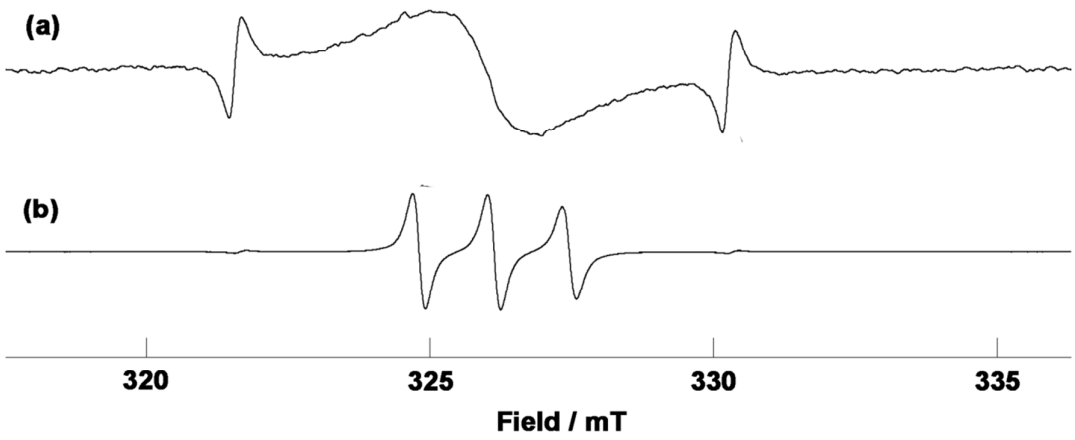

Fig. 9 (a) EPR spectra of (*S*,*S*,*R*)-**5a** (1.0 x 10^{-4} mol/L) in H_2O at 25 °C. (b) EPR spectra of (*S*,*S*,*R*)-**5a** (1.0 x 10^{-2} mol/L) in THF at 25 °C.

From these results, the gelation process is most likely to involve (1) formation of 1D chains of (*S*,*S*,*R*)-**5a** through the hydrogen bond between the amide oxygen atom and the carboxylic acid, (2) growth of 2D nanosheet by supramolecular assembly of the 1D chains by hydrophobic interactions of long alkyl chains (Fig. 6c), (3) formation of nanofibers by stacking of 2D nanosheets, (4) entanglement of the nanofibers to create 3D networks, and (5) trapping of water molecules in the inner space of the 3D networks by the surface tension.[43-45]

3.2 Magnetic behavior

Although the gel–sol transition temperature of (*S*,*S*,*R*)-**5a** could not be determined by DSC analysis, it was assumed to be around 32 °C by using the standard test-tube inversion methods (Fig. 3).[24] To confirm this transition point and gain an insight into the change in the magnetic behavior between the gel and sol states, the temperature dependence of EPR spectra was measured for the hydrogel sample (3.4 wt%) loaded in a glass capillary (<1 mm ϕ) in a temperature range between 27 °C and 55 °C at a magnetic field of 0.33 T (X-band, at a fixed frequency with sweeping field centered at 0.33 T) (Fig. S4). The EPR peak-to-peak line-width (ΔH_{pp}) and *g*-value were directly determined from the spectra, and the *g*-values were in good agreement with those obtained by the satisfactory line shape simulation of the spectral data using the EasySpin program (Fig. S5, Table S1)[46,47] based on the convolution of Gaussian with

Soft Matter Accepted Manuscript

Lorentzian functions.[48] No appreciable change in the *g*-value was noted in both heating and cooling runs (Fig. S6), indicating almost no change in the molecular orientation between the gel and sol states. On the contrary, ΔH_{pp} increased at the gel-to-sol transition and then gradually decreased in the heating run (Fig. 10). Generally the increase in ΔH_{pp} reflects either of the following two magnetic interactions; (a) an increase in spin-spin dipole interaction or (b) a decrease in spin-spin exchange interaction. Since the entangled nanofibers collapse to form colloidal solution at the gel-to-sol transition, the decreased spin-spin exchange interaction should be responsible for the increase in ΔH_{pp}, followed by the gradual decrease in ΔH_{pp} due most likely to the motional narrowing. A similar tendency was observed in the cooling run. Thus, it should be noted that EPR spectroscopy is an excellent tool for determining the transition temperature and evaluating the intermolecular spin-spin interactions.

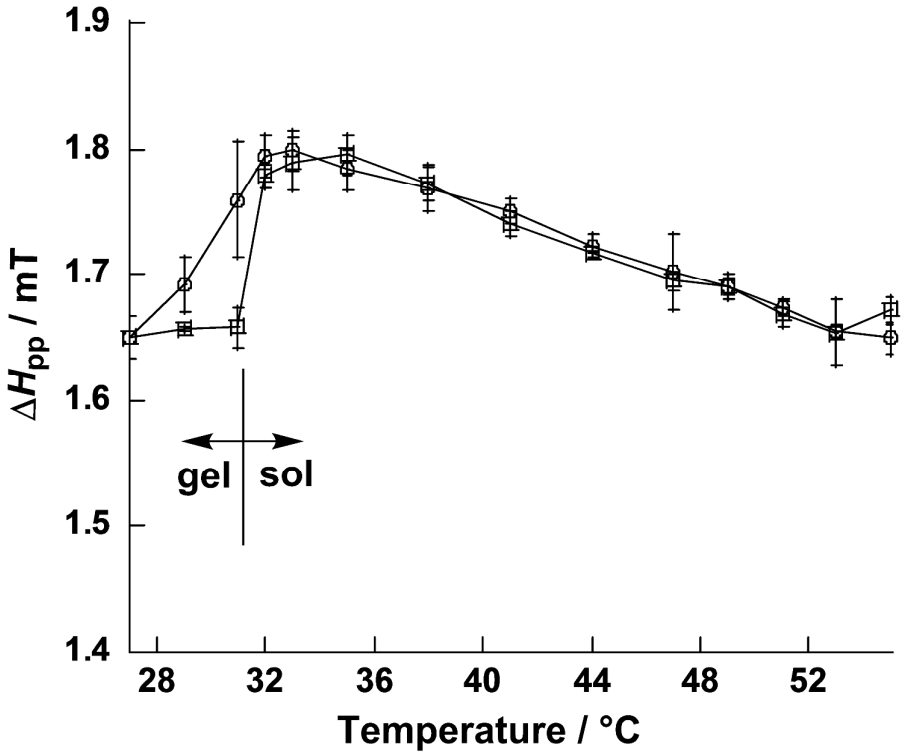

Fig. 10 Temperature dependence of peak-to-peak line-width (ΔH_{pp}) in the gel and sol states of (*S*,*S*,*R*)-**5a**. Circles and squares indicate the data in the first cooling and second heating runs, respectively.

Next, to evaluate the temperature dependence of paramagnetic susceptibility (χ_{para}) in the gel and sol states, the relative paramagnetic susceptibility (χ_{rel}) which is defined

Soft Matter Accepted Manuscript

as

$$\chi_{\text{rel}} = \frac{\chi_{\text{para}}}{\chi_0} \qquad (1)$$

where χ_0 is the standard paramagnetic susceptibility (equal to the double integral of an EPR spectrum) at 27 °C, was employed. This is because it is difficult to evaluate the χ_{para} value accurately by SQUID measurement of the hydrogel containing only 3.4 wt% of (*S*,*S*,*R*)-**5a** at high temperatures. The mean χ_{rel} values of three measurements at each temperature were plotted along with the standard deviation represented by error bars (Fig. 11). At the gel–to–sol transition, no appreciable change was noted. As the temperature increased, the χ_{rel} decreased gradually according to the Curie-Weiss law. Since the χ_{para} –T plot for the xerogel of (*S*,*S*,*R*)-**5a** at 0.05 T obtained by SQUID measurements obeyed the Curie–Weiss law in the temperature range of 2 K to 300 K (Weiss constant θ = –0.28 K and Curie constant C = 0.342 emu K mol^{-1}), exhibiting a paramagnetic behavior below 300 K (Fig. S7 and Table S2), it is natural to consider that the spins are under the paramagnetic circumstance in both the gel and sol states, too.

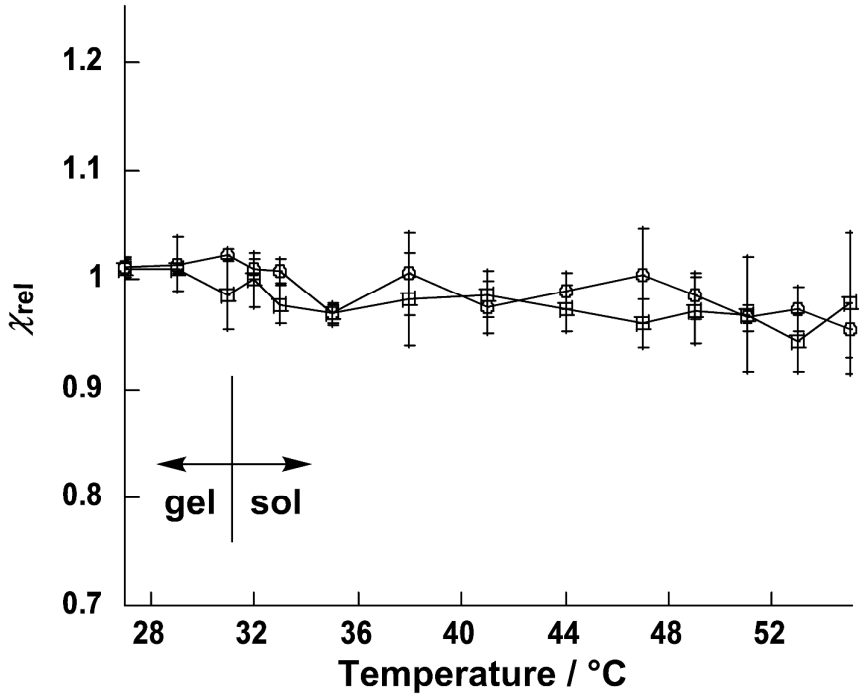

Fig. 11 Temperature dependence of χ_{rel} in the gel and sol phases for (*S*,*S*,*R*)-**5a**. Circles denote the first cooling run, while squares represent the second heating run.

4 Conclusions

Soft Matter Accepted Manuscript

For the first time, a spin-labelled physical hydrogel containing a chiral cyclic nitroxide radical unit fixed in the inner position of a low-molecular-weight gelator molecule was prepared. The dynamic behavior of the chiral radical hydrogelator (*S*,*S*,*R*)-**5a** ($\Delta\varepsilon < 0$) in the gel and sol states was evaluated by VT-EPR spectroscopy. The gel–sol transition temperature was accurately determined by EPR spectral line-width analysis. For the measurement of the temperature dependence of paramagnetic susceptibility (χ_{para}) at high temperatures for the hydrogel and sol phases containing a small amount of organic radical gelator in H_2O, the relative paramagnetic susceptibility (χ_{rel}) obtained by means of the double-integration of EPR spectra was employed. Consequently, no appreciable change in the intermolecular magnetic interactions between the gel and sol states was noted. In addition, the present method will be used as a convenient and reproducible, general tool to evaluate the change in magnetic interactions at a phase transition in nitroxide radical-labelled soft materials at high temperatures in place of SQUID measurement.

Acknowledgements

We thank Professor Nobuyuki Harada for helpful advice on our UV and CD spectroscopic experiments. The present work was supported by JSPS KAKENHI (Grant numbers 23245008 and 26248024). The TEM experiment was carried out by using a facility in the Research Center for Ultrahigh Voltage Electron Microscopy, Osaka University. The SAXS measurement was performed under the approval of the Photon Factory Program Advisory Committee (Proposal No. 2014G127 and 2014G162).

References

1 H. G. Aurich in *Nitrones, Nitronates and Nitroxides* (Eds.: E. Breuer, H. G. Aurich, A. Nielsen,), John Wiley & Sons, Chichester, **1989**, pp. 313-370.

2 M. Tamura, Y. Nakazawa, D. Shiomi, K. Nozawa, Y. Hosokoshi, M. Ishikawa, M. Takahashi, M. Kinoshita, *Chem. Phys. Lett.* **1991**, *186*, 401-404.

3 P. M. Lahti, *Adv. Phys. Org. Chem.* **2011**, *45*, 93-169.

4 T. Sugawara, H. Komatsu, K. Suzuki, K. *Chem. Soc. Rev.* **2011**, *40*, 3105-3118.

5 *Stable Radicals: Fundamental and Applied Aspects of Odd-electron Compounds* (Ed.: R. Hicks), John Wiley & Sons, Chichester, **2010**.

6 G. I. Likhtenshtein, J. Yamauchi, S. Nakatsuji, A. I. Smirnov, R. Tamura, *Nitroxides: Applications in Chemistry, Biomedicine, and materials Science*, Wiley-VCH, Weinheim, **2008**.

7 *Magnetism: Molecules to Materials, Vol. 1-5* (Eds.: J. S. Miller, M. Drillon),

Soft Matter Accepted Manuscript

Wiley-VCH, Weinheim, **2001-2005**.
8 K. Itoh, M. Kinoshita, *Molecular Magnetism New Magnetic Materials*, Kodansha Gordon and Breach Science Publishers, Tokyo, **2000**.
9 *Magnetic Properties of Organic Materials* (Ed.: P. M. Lahti), Marcel-Dekker, New York, **1999**.
10 Amabilino, D. B.; Veciana, J. in *Magnetism: Molecules to Materials II* (Eds.: Miller, J. S.; Drillon, M.), Wiley-VCH, Weinhiem, **2001**, pp. 1-60.
11 R. Chiarelli, M. A. Novak, A. Rassat, J. L. Tholence, *Nature*, **1993**, 363, 147-149.
12 R. Tamura, Y. Uchida, K. Suzuki in *Hadbook of Liquid Crystals, Second Edition* (Eds.: J. W. Goodby, P. J. Collings,T. Kato, C. Tschierske, H. F. Gleeson, P. Raynes), Wiley-VCH, Weinheim, **2014**, Vol. 8, pp. 837-864.
13 R. Tamura, K. Suzuki, Y. Uchida, Y. Noda, *Electron Paramag. Reson*. **2013**, *23*, 1-21.
14 Bardelang, M. Hardy, O. Ouari, P. Tordo in *Encyclopedia of Radicals in Chemistry, Biology and Materials, Vol.4 Polymers and Materials* (Eds: C. Chatgilialoglu, A. Studer), John Wiley & Sons, Chichester, **2012**, pp. 1965-2015.
15 R. Tamura, Y. Uchida, K. Suzuki in *Liquid Crystals Beyond Display: Chemistry, Physics, and Applications* (Ed.: Q. Li), John Wiley & Sons, Hoboken, **2012**, pp. 83-110.
16 R. Tamura, Y. Uchida, K. Suzuki in *Nitroxides: Theory, Experiment and Applications* (Ed.: A. I. Kokorin), InTech, Rijeka, Croatia, **2012**, pp. 191-210.
17 R. Tamura, Y. Uchida, N. Ikuma, *J. Mater. Chem.* **2008**, *18*, 2872-2876.
18 Y. Uchida, N. Ikuma, R. Tamura, S. Shimono, Y. Noda, J. Yamauchi, Y. Aoki, H. Nohira, *J. Mater. Chem.* **2008**, *18*, 2872-2876.
19 Y. Uchida, K. Suzuki, R. Tamura, N. Ikuma, S. Shimono, Y. Noda, J. Yamauchi, *J. Am. Chem. Soc.* **2010**, *132*, 9746-9752.
20 K. Suzuki, Y. Uchida, R. Tamura, S. Shimono, J. Yamauchi, *J. Mater. Chem.* **2012**, *22*, 6799-6806.
21 Y. Uchida, K. Suzuki, R. Tamura, *J. Phys. Chem. B* **2012**, *116*, 9791-9795.
22 K. Suzuki, Y. Uchida, R. Tamura, Y. Noda, N. Ikuma, S. Shimono. J. Yamauchi, *Soft Matter* **2013**, *9*, 4687-4692.
23 A. Kh. Vorobiev, N. A. Chumakova, D. A. Pomogailo, Y. Uchida, K. Suzuki, Y. Noda, R. Tamura, *J. Phys. Chem. C*, **2014**, *118*, 1932-1942.
24 *Molecular Gels: Materials with Self-Assembled Fibrillar Networks* (Eds.: R. G. Weiss, P. Terech), Springer, Dordrecht, **2006**.
25 *Low Molecular Mass Gelators: Design, Self-Assembly, Function* (Ed.: F. Fages), *Topics in Current Chemistry*, Vol. 256, Springer, Heidelberg, **2005**.

Soft Matter Accepted Manuscript

26 L. A. Estroff, A. D. Hamilton, *Chem. Rev.* **2004**, *104*, 1201-1217.
27 P. Terech, R. G. Weiss, *Chem. Rev.* **1997**, *97*, 3133-3159.
28 P. Terech, R. Ramasseul, F. Volino, *J. Colloid Interface Sci.* **1983**, *91*, 280-282.
29 Y. Wu, Y. Hirai, Y. Tsunobuchi, H. Tokoro, H. Eimura, M. Yoshio, S. Ohkoshi, T. Kato, *Chem. Sci.* **2012**, *3*, 3007-3010.
30 M. Mannini, S. Cicchi, D. Berti, A. Caneschi, A. Brandi, L. Lascialfari, L. Sorace, *ChemPlusChem* **2013**, *78*, 149-156.
31 G. Ionita, A. M. Ariciu, I. M. Turcu, V. Chechik, V. *Soft Matter* **2014**, *10*, 1778-1783.
32 A. Altomare, M. Burla, M. Camalli, G. Cascarano, C Giacovazzo, A. Guagliardi, A. Moliterni, G. Polidori, R. Spagna, *J. Appl. Crystallogr.* **1999**, *32*, 115–119.
33 G. M. Sheldrick, *Acta Cryst*. **2008**, *A64***,** 112–122.
34 C. Kabuto, S. Akine, T. Nemoto, E. Kwon, *J. Cryst. Soc. Jpn.* **2009**, *51*, 218-224.
35 Y. Uchida, R. Tamura, N. Ikuma, J. Yamauchi, Y. Aoki, H. Nohira, *Ferroelectrics* **2008**, *365*, 158-169.
36 Y. Uchida, R. Tamura, N. Ikuma, S. Shimono, J. Yamauchi, Y. Aoki, H. Nohira, *Mol. Cryst. Liq. Cryst.* **2007**, *479*, 213-221.
37 Y. Uchida, T. Uematsu, Y. Nakayama, Y.; Takahashi, H.; Tsue, H.; Tanaka, K.; Tamura, R. *Chirality* **2008**, *20*, 282-287.
38 J. Fuhrhop, P. Schnieder, E. Boekema, W. Helfrich, *J. Am. Chem. Soc.*, **1988**, 110, 2861-2867
39 Y. Li, F. Zhou, Y. Wen, K. Liu, L. Chen, Y. Mao, S. Yang, T. Yi, *Soft Matter*, **2014**, 10, 3077-3085.
40 S. Kabashima, M. Kageyama, T. Okano, I. Yoshikawa, K. Araki, *J. Colloid. Interface. Sci*., **2013**, 408, 107-112.
41 *Circular Dichroism*: *Principles and Applications*, *Second Edition* (Eds.: N. Berova, K. Nakanishi, R. W. Woody), Wiley-VCH, New York, **2000**.
42 J. R. Platt, *J. Chem. Phys.* **1949**, *17*, 484-495.
43 A. Keller, *Faraday Discuss*. **1995**, *101*, 1-49.
44 R. Wang, C. Geiger, L. Chen, B. Swanson, D. G. Whitten, *J. Am. Chem. Soc*. **2000**, 122, 2399-2400.
45 K. Sakurai, Y. Jeong, K. Koumoto, A. Friggeri, O. Gronwald, S. Sakurai, S. Okamoto, K. Inoue, S. Shinkai, *Langmuir* **2003**, 19, 8211-8217.
46 http://www.easyspin.org/
47 S. Stoll, A. Schweiger, *J. Magn. Reson.* **2006**, *178*, 42-55.
48 A. Cabral-Prieto, H. Jimemez-Dominguez, L. Gonzalez-Tovany, S. Galindo, H. Flores-Llamas, M. Torres-Valderrama. *J. Magn. Reson.***1990**, *89*, 568-571.

Soft Matter Accepted Manuscript